

**THE DYING-WIND AROUND HD 56126, A POST-AGB  
CARBON STAR**

M. Jura and C. Chen

Department of Physics and Astronomy, University of California, Los Angeles CA  
90095-1562; jura@clotho.astro.ucla.edu; cchen@astro.ucla.edu

and

M. W. Werner

Jet Propulsion Laboratory, 264-767, 4800 Oak Grove Dr., Pasadena CA 91109;  
mwerner@sirtfweb.jpl.nasa.gov

Received \_\_\_\_\_; accepted \_\_\_\_\_

## ABSTRACT

We have used the Keck I telescope to resolve at mid-infrared wavelengths the dust emission from HD 56126 (IRAS 07134+1005), a post-Asymptotic Giant Branch carbon star with a detached dust shell. The gross morphology of the image can be explained by a strong wind which started to die about 1500 years ago. If the star had an effective temperature,  $T_*$ , near 2600 K when it was losing  $\sim 3 \times 10^{-5} M_{\odot} \text{ yr}^{-1}$ , then during the past 1500 yr, the average value of  $dT_*/dt$  has been  $+2.2 \text{ K yr}^{-1}$ . With such a time variation of the effective temperature, the  $11.7 \mu\text{m}$  image can be approximately reproduced if the mass loss rate varied as  $T_*^{-8.26}$ , as proposed in recent models for dust-driven winds. Since the mass loss rate appears to be very sensitive to the effective temperature of the star, we speculate that the observed deviations from spherical symmetry of the dust shell can be explained by plausible variations in the surface temperature of the mass-losing star caused by rotation and/or magnetic fields.

*Subject headings:* stars: AGB and post-AGB; circumstellar matter; winds-outflows

## 1. INTRODUCTION

Mass loss with rates near  $\sim 10^{-5} M_{\odot} \text{ yr}^{-1}$  during the Asymptotic Giant Branch (AGB) phase is important both in the evolution of the mass-losing star and in replenishing the interstellar medium (see, for example, Habing 1996). After a star evolves off the AGB, its effective temperature rises, its radius shrinks and the wind dies (Vassiliadis & Wood 1993, Blocker 1995, Schroder, Winters & Sedlmayr 1999).

Stars slightly beyond the end of their AGB evolution can be identified by having only relatively cold dust since they are no longer losing much mass. Therefore, they exhibit a large infrared excess but with dust temperatures typically less than 200 K (see, for example, Kwok 1993). The detached dust shell can be extended over the sky and thus provide the opportunity to examine the history of the star’s mass loss.

Meixner et al. (1997, 1999) and Dayal et al. (1998) have acquired mid-infrared images and resolved more than 10 post-AGB stars or “transition objects”. Even in the best-studied cases, the angular diameter of the dust emission is not much larger than the characteristic  $0''.9$  angular resolution available at the 4m-class telescopes used for these previous studies. With the 10m Keck telescope, it is possible to achieve significantly higher angular resolution (see, for example, Jura & Werner 1999, Jura, Chen & Werner 2000) and thus develop more exacting tests of models for dying winds.

Here, we report the result of using Keck to obtain mid-IR images of HD 56126 ( $m_V = 8.27$  mag, spectral type F5I), a post-AGB carbon star with a nebula displaying one of the largest angular sizes in the sample studied by Meixner et al. and extended optical reflection nebulosity as well (Ueta, Meixner & Bobrowsky 2000). This star is also a “ $21 \mu\text{m}$ ” source (see, for example Kwok, Volk & Hrivnak 1999), a feature attributed to TiC (von Helden et al. 2000). In Section 2 we present our observations while in Section 3, we describe our estimates for the physical properties of the circumstellar envelope and the central star. In

section 4, we present a model to explain the gross features of the system while in Section 5, we discuss models to explain deviations from a spherically symmetric wind. In Section 6 we present our conclusions.

## 2. OBSERVATIONS

Our data were obtained on the night 2000 Feb 20 (UT) at the Keck I telescope using the Long Wavelength Spectrometer (LWS) which was built by a team led by B. Jones and is described on the Keck web page. The LWS uses a  $128 \times 128$  SiAs BIB array with a pixel scale at the Keck telescope of  $0''.08$  and a total field of view of  $10''.2 \times 10''.2$ . We used the “chop-nod” mode of observing, and 4 different filters:  $7.5 - 8.2 \mu\text{m}$ ,  $9.4-10.2 \mu\text{m}$ ,  $11.2 - 12.2 \mu\text{m}$  and  $18.4-18.9 \mu\text{m}$ . We used  $\alpha$  Boo for flux and point-spread-function calibrations. The data were reduced at UCLA using standard LWS routines.

The image in the  $11.7 \mu\text{m}$  filter is presented in Figure 1; the images at other wavelengths appear similar. Probably because of our higher angular resolution, our measured peak surface brightness of  $4.0 \text{ Jy arcsec}^{-2}$  is greater than the peak values of  $2.3 \text{ Jy arcsec}^{-2}$  and  $3.0 \text{ Jy arcsec}^{-2}$  found by Meixner et al. (1997) and Dayal et al. (1998), respectively. Given the  $\sim 10\%$  uncertainties in our data, our measured flux at  $11.7 \mu\text{m}$  of  $28 \text{ Jy}$  is consistent with the values for the flux of  $30 \pm 3 \text{ Jy}$  (Dayal et al. 1998),  $25.7 \pm 2.6 \text{ Jy}$  (Meixner et al. 1997)  $25 \pm 3 \text{ Jy}$  (Justtanont et al. 1996) and  $25 \text{ Jy}$  (IRAS).

Beyond  $1''.5$  from the center of the nebula, the isophotes are smooth and elliptically shaped with the major axis lying near Position Angle  $45^\circ$  and being about  $7\%$  greater than the minor axis. A hint of ellipticity at this position angle is also seen in the mid-IR images of Meixner et al. (1997) and Dayal et al. (1998) as well as in the optical reflection nebulosity presented by Ueta et al. (2000). In the inner  $1''.5$  there is a marked change in

the morphology of the dust with two bright blobs lying near the minor axis of the ellipse defined by the outer contours. The bright blob at about  $1''$  to the southeast of the center of the image is seen in the data presented both by Dayal et al. (1998) and Meixner et al. (1997). The maximum intensity in the bright blob is about a factor of 1.5 greater than the maximum intensity in the faint blob. Our image at  $8\mu\text{m}$  shows that HD 56126 lies within  $\pm 0''.2$  of the center of the dust ring defined by the outer, elliptical isophotes.

### 3. STELLAR AND CIRCUMSTELLAR PARAMETERS

The observed pulsation properties of HD 56126 can be used to place the star in the H-R diagram and to estimate its mass. Since HD 56126 is variable with a period of 36.8 days (Barthes et al. 2000), it is plausible that the mass of the star is near  $0.6 M_{\odot}$  and the time-averaged luminosity is near  $6600 L_{\odot}$  (Tuchman et al. 1993, Jeannin et al. 1997, Barthes et al. 2000). From the observed time-averaged flux (see Meixner et al. 1997), we therefore infer a distance of 2300 pc. The time-averaged effective temperature,  $T_*$ , and radius,  $R_*$ , are 5900 K and  $5.5 \times 10^{12}$  cm, respectively (Barthes et al. 2000). Although carbon, nitrogen and oxygen have nearly solar abundances, since the iron group elements have abundances about 0.1 of solar (Parthasarathy, Garcia Lario & Pottasch 1992, Klochkova 1995, Van Winckel & Reyniers 2000), HD 56126 probably is a member of the thick disk and its main sequence progenitor probably had a mass near  $1.1 M_{\odot}$ . Therefore, it is likely that HD 56126 has already experienced a total mass loss of  $0.5 M_{\odot}$ . Evidence that HD 56126 is a post-AGB star is provided by the greater than solar abundance of the s-process elements such as Sr, Y, Zr and Ba.

Below, we propose that  $\sim 1500$  years ago, HD 56126 was losing  $\sim 3 \times 10^{-5} M_{\odot} \text{ yr}^{-1}$ . In this phase, its effective temperature was probably near 2600 K (Arndt et al. 1997). Therefore, during the past 1500 yr, the average value of  $dT_*/dt$  has been  $+2.2 \text{ K yr}^{-1}$ .

The star probably maintained a constant luminosity during its post-AGB evolution (see, for example, Vassiliadis & Wood 1993) so that as the temperature increased, the radius decreased from  $2.8 \times 10^{13}$  cm to its current value.

Although, as inferred from the profile of the CO (2-1) circumstellar emission line, most of the gas outflow is at  $10.7 \text{ km s}^{-1}$  (Knapp et al. 1998), there are significant deviations from this value. Crawford & Barlow (2000) have obtained optical spectra with a resolution of 860,000, and they found three distinct components in the K I circumstellar shell lines with a net spread in the velocity of the circumstellar gas of  $2 \text{ km s}^{-1}$ .

#### 4. THE SPHERICALLY SYMMETRIC WIND

To compute the surface brightness,  $I_\nu$ , of the nebulosity, we numerically determine:

$$I_\nu = \int \chi_\nu \rho(D) B_\nu(T_{gr}) ds \quad (1)$$

where  $B_\nu$  is the Planck function,  $ds$  is the increment of distance along the line of sight,  $\rho(D)$  is the dust density at distance,  $D$ , from the star and the dust opacity is  $\chi_\nu$ . To compute the dust temperature as a function of the distance, we follow Sopka et al. (1985) and assume that the dust grains are heated by the light from the central star and re-radiate in the infrared. For carbon-rich particles, we adopt a simple model for the grain opacity,  $\chi_\nu$  ( $\text{cm}^2 \text{ g}^{-1}$ ) such that

$$\chi_\nu = \chi_{\nu_0} (\nu/\nu_0)^{1.3} \quad (2)$$

with  $\chi_{\nu_0} = 150 \text{ cm}^2 \text{ g}^{-1}$  at  $\nu_0 = 5 \times 10^{12} \text{ Hz}$  ( $60 \text{ } \mu\text{m}$ ) (Le Bertre 1997). When the circumstellar envelope is optically thin, the dust grain temperature,  $T_{gr}$ , can be written as:

$$T_{gr} = 0.77 T_* (R_*/D)^{0.38} \quad (3)$$

With this prescription,  $T_{gr}$  at  $1''$  from the central star is 170 K while Meixner et al. (1997) and Dayal et al. (1998) inferred values of 160 K and 185 K, respectively. For  $11.7 \text{ } \mu\text{m}$

photons,  $h\nu/k = 1230$  K, and therefore the nebulosity is produced by grains emitting on the Wien portion of the Planck curve.

To compute  $\rho(D)$ , we assume a spherically symmetric envelope where the dust outflow velocity,  $V_{gr}$ , does not change with time. We assume that the mass loss rate of grains,  $\dot{M}_{gr}(t)$ , and  $T_*$  were constant until a moment came when the star’s effective temperature started to increase and the wind started to die. During the dying-wind phase, we assume that  $dT_*/dt$  was constant. The current boundary between the zone where the wind had a constant mass loss rate and where it started to die, lies at a distance  $D_{die}$  with  $D_{die} = V_{gr} t_{die}$ . Here,  $t_{die}$  denotes the amount of time that has elapsed since that moment when the star’s effective temperature began to increase. From the equation of continuity and the simple mapping between the dust travel time,  $t_{travel}$ , and distance from the star, then:

$$\rho_{gr}(D) = \dot{M}_{gr}(t_{travel}) / (4\pi V_{gr} D^2) \quad (4)$$

In the models for mass loss from carbon-rich AGB stars by Arndt et al. (1997),  $\dot{M}_{gr}$  varies as  $T_*^{-8.26}$ . Such a steep variation of the mass loss with temperature occurs because the mass loss rate is controlled by radiation pressure on grains, and the dust formation is very sensitive to the gas temperature.

The best fit to the  $11.7 \mu\text{m}$  image shown in Figure 1 is with a model derived from equation (1) where  $D_{die} = 5 \times 10^{16}$  cm, corresponding to an angular radius of  $1''.5$  or  $t_{die} = 1500$  yr, and  $dT_*/dt = +2.2$  K yr $^{-1}$ . We show in Figure 2 the results of comparing the results from this model with transverse cuts through the intensity data at  $11.7 \mu\text{m}$ . In the region where  $D < D_{die}$ , the projected  $11.7 \mu\text{m}$  intensity depends upon the multiplication of two rapidly varying quantities: the mass loss rate and the Wien portion of the Planck function. The qualitative agreement between our data and the observations lends support to the dying wind model, but other possible models for  $\dot{M}(t)$  are not excluded by our observations.

At  $1''.5$  from the star, the  $11.7 \mu\text{m}$  intensity of the nebula is about  $2.0 \text{ Jy arcsec}^{-2}$ . Therefore, in the outer region,  $\dot{M}_{gr} = 1.7 \times 10^{-7} M_{\odot} \text{ yr}^{-1}$ . Although uncertain, a dust to gas ratio of  $5 \times 10^{-3}$  is plausible and therefore the total mass loss rate before the wind started to die was  $\sim 3 \times 10^{-5} M_{\odot} \text{ yr}^{-1}$ . Given the uncertainties in the distance to the star, the dust to gas ratio, the emissivity of the grains and the observations that there is an appreciable amount of carbon in C I as well as CO (Bakker et al. 1996, Bakker & Lambert 1998, Knapp et al. 2000), this estimate of the mass loss rate for the phase just before the winds dies is consistent with previous estimates by Hrivnak et al. (1989), Meixner et al. (1997) and Dayal et al. (1998).

## 5. DISCUSSION

As a first approximation, much of our data can be explained in terms of a nearly-spherical wind of  $\sim 3 \times 10^{-5} M_{\odot} \text{ yr}^{-1}$  which started to die about 1500 yr ago, consistent with models for post-AGB evolution of carbon-rich stars (Vassiliadis & Wood 1993, Blocker 1995, Schroder et al. 1999).

In order to produce a high enough pressure in the outflow to manufacture TiC, von Helden et al. (2000) proposed a short-lived phase with a steady-state mass loss rate of  $10^{-3} M_{\odot} \text{ yr}^{-1}$  which is not supported by our data. Nevertheless, models for shock-driven mass loss from AGB stars may possibly explain the presence of TiC around HD 56126. In calculations by Winters et al. (1997) for a carbon star with a time-averaged mass loss rate of  $1.2 \times 10^{-4} M_{\odot} \text{ yr}^{-1}$ , as shown in their Figure 2, at 2 stellar radii above the star, the density can be as high as  $10^{-11} \text{ g cm}^{-3}$  when the gas temperature is 1800 K. Therefore, the gas pressure can be  $\sim 1 \text{ dyne cm}^{-2}$  at a temperature nearly low enough to produce solid TiC (Bernatowicz et al. 1996). There may have been phases during the pulsational cycle of HD 56126 while it was on the AGB when the physical conditions were favorable for the



production of the apparent carrier of the 21  $\mu\text{m}$  emission feature even if the mass loss rate was as “low” as  $3 \times 10^{-5} M_{\odot} \text{ yr}^{-1}$ .

The nebula shows significant deviations from spherical symmetry. Because the mass loss rate is extremely sensitive to the photospheric temperature, we tentatively explore the possibility that deviations from spherical symmetry in the dust shell can be explained by temperature variations on the surface of the star while it was losing mass.

### 5.1. The Outer Ellipticity

As can be seen in Figure 1, beyond  $1''.5$  from the center, for a given distance from the center, the intensity at position angle  $45^{\circ}$  is greater than at, say, position angle  $135^{\circ}$ . From equation (1), if the grain opacity is the same throughout the nebula, then these data can be reproduced either by variations in  $\rho$  or by variations in  $T_{gr}$ . The 18.7  $\mu\text{m}$  image displays the same ellipticity as does the 11.7  $\mu\text{m}$  image so that azimuthal variations in the temperature do not seem to explain the variations in the intensity. Instead, we propose that there are more grains at position angle  $45^{\circ}$  than at position angle  $135^{\circ}$  and thus that there was more mass loss directed toward position angle  $45^{\circ}$ .

If the star is rotating and there is enhanced mass loss at the equatorial bulge (Dorfi & Hofner 1996, Soker 1998, Reimers, Dorfi & Hofner 2000), then qualitatively, the data can be explained if the rotation axis is projected along position angle  $135^{\circ}$ . If  $\dot{M}$  varies as  $T_*^{-8.26}$  then a 1% variation in the temperature can lead to an 8% variation in the mass loss rate – a change great enough to explain the observed 7% ellipticity in the isophotes.

If the surface of the star is an equipotential, if the star rotates as a solid body with angular velocity  $\omega_*$ , and if  $\theta$  denotes the co-latitude, then:

$$(1/2)\omega_*^2 R_*(\theta)^2 \sin^2 \theta + GM_*/R_*(\theta) = \text{constant} \quad (5)$$

When the star was on the AGB with  $T_* = 2600$  K,  $\bar{R}_* = 2.8 \times 10^{13}$  cm and  $M = 0.6 M_\odot$ , and if  $R_{eq}/R_{pole}$  was  $\sim 1.02$ , consistent with a temperature contrast between the poles and equator of 1.01 and the assumption that  $R^2 T_*^4$  is constant over the surface of the star, then  $\omega_*$  was approximately  $1 \times 10^{-8} \text{ s}^{-1}$ . The angular momentum of the rotating AGB star was approximately  $2/9 M_* R_*^2 \omega_*$  (Soker 1998) or  $2 \times 10^{51} \text{ g cm}^2 \text{ s}^{-1}$ . It is plausible that HD 56126 could have acquired this angular momentum if, when it first swelled onto the AGB, it engulfed a putative  $0.1 M_\odot$  companion in a circular orbit at 1 AU which would then have donated  $9 \times 10^{51} \text{ g cm}^2 \text{ s}^{-1}$  of angular momentum. An example of a carbon star that has probably engulfed a companion and acquired such a large amount of angular momentum is V Hya (Barnbaum, Morris & Kahane 1995, Kahane et al. 1996). However, we have no evidence in support of the proposed magnitude or orientation of the rotation of HD 56126, and our hypothesis to explain the observed ellipticity is quite tentative.

## 5.2. The Inner Blobs

Meixner et al. (1997) propose that the bright blobs are the consequence of an equatorially-enhanced ejection. Their model implies that the position angle of the rotation axis lies near  $45^\circ$ ; a very different orientation from what we propose. One difficulty with the model by Meixner et al. (1997) is that the southeastern blob is considerably brighter than the northwestern blob. However, it is possible that the bright blob is a factor of 1.2 closer to the central star than the faint blob, and this could explain the intensity difference between the two blobs. An offset of the central star from the center of the nebula could occur if the system is a wide binary as apparently occurs in TT Cyg (Olofsson et al. 2000).

If, as we propose above, the position angle of the rotation axis is  $135^\circ$ , then another model besides that of Meixner et al. (1997) is required to explain the existence of the bright blobs. One possibility is that as the star first evolved away from the AGB, the

magnetic field was strongest at the rotational poles with the consequence that the gas was particularly cold in these regions. We speculate that the mass loss continued from the poles for 500 years after it had greatly diminished from the equator. If the field were stronger at one pole than the other, then the two blobs in the nebula could have different intensities. To appreciably change the surface temperature of the star, the energy density in the magnetic field,  $B^2/(8\pi)$  must be comparable to the thermal pressure in the photosphere (Soker & Clayton 1999). The required value of the magnetic field is therefore  $[(16\pi g)/(3\chi)]^{1/2}$  where  $\chi$  is the Kramers opacity in the atmosphere or  $\sim 3 \times 10^{-3} \text{ cm}^2 \text{ g}^{-1}$  (Soker 1998) and  $g$  is the gravitational acceleration which was near  $0.1 \text{ cm s}^{-2}$  when the star was just leaving the AGB. Thus a field of  $\sim 20$  Gauss is implied. From VLBA maps of polarized SiO masers, magnetic fields approaching this amplitude have been inferred around the oxygen-rich Mira variable TX Cam (Kemball & Diamond 1997), but the true value of the magnetic field is controversial and may be only 0.03 Gauss (Wiebe & Watson 1998, Desmurs et al. 2000).

## 6. CONCLUSIONS

We have obtained high-resolution mid-IR images of the detached dust shell around the carbon star HD 56126 and propose the following:

1. The gross features of the region beyond a radius of  $1''.5$  can be reproduced by an approximately spherical wind from a star which had a mass loss rate of  $\sim 3 \times 10^{-5} M_{\odot} \text{ yr}^{-1}$  while it was on the AGB. After the star left the AGB, its effective temperature increased with an average rate of  $+2.2 \text{ K yr}^{-1}$  and the mass loss rate varied as  $T_*^{-8.26}$ , as expected in models for dust-driven winds.

2. The extreme sensitivity of the mass loss rate to the effective temperature of the star allows us to tentatively propose that both the ellipticity in the outer envelope and the inner

blobs can be explained by plausible temperature variations on the surface of the star which might have resulted from rotation and/or large scale magnetic fields.

We thank M. Meixner for a particularly thoughtful referee’s report and M. Morris for his comments. This work has been partly supported both at UCLA by NASA and at the Jet Propulsion Laboratory, California Institute of Technology, under an agreement with NASA.

## REFERENCES

- Arndt, T. U., Fleischer, A. J. & Sedlmayr, E. 1997, *A&A*, 327, 614
- Bakker, E. J., Waters, L. B. F. M., Lamers, H. J. G. L. M., Trams, N. R., & van der Wolf, F. L. A. 1996, *A&A*, 310, 893
- Bakker, E. J. & Lambert, D. L. 1998, *ApJ*, 508, 387
- Barnbaum, C., Morris, M., & Kahane, C. 1995, *ApJ*, 450, 826
- Barthes, D., Lebre, A., Gillet, D. & Mauron, N. 2000, *A&A*, 359, 168
- Bernatowicz, T. J., Cowsik, R., Gibbons, P., Lodders, K., Fegley, B., Amari, S. & Lewis, R. S. 1996, *ApJ*, 472, 760
- Blocker, T. 1995, *A&A*, 297, 727
- Crawford, I. A. & Barlow, M. J. 2000, *MNRAS*, 311, 370
- Dayal, A., Hoffmann, W. F., Biegging, J. H., Hora, J. L., Deutsch, L. K., & Fazio, G. G. 1998, *ApJ*, 492, 603
- Desmurs, J. F., Bujarrabal, V., Colomer, F. & Alcolea, J. 2000, *A&A*, 360, 189
- Dorfi, E. A. & Hofner, S. 1996, *A&A*, 313, 605
- Habing, H. 1996, *A&AR* 7, 97
- Hrivnak, B. J., Kwok, S. & Volk, K. M. 1989, *ApJ*, 346, 265
- Jeannin, L., Fokin, A. B., Gillet, D. & Baraffe, I. 1997, *A&A*, 326, 203
- Jura, M. & Werner, M. W. 1999, *ApJ*, 525, L113
- Jura, M., Chen, C. & Werner, W. W. 2000, *ApJ*, 541, 264

- Justtanont, K., Barlow, M. J., Skinner, C. J., Roche, P. F., Aitken, K. & Smith, C. H. 1996, *A&A*, 309, 612
- Kahane, C., Audinos, P., Barnbaum, C. & Morris, M. 1996, *A&A*, 314, 871
- Kemball, A. J. & Diamond, P. J. 1997, *ApJ*, 481, L111
- Klochkova, V. G. 1995, *MNRAS*, 272, 710
- Knapp, G. R., Crosas, M., Young, K. & Ivezić, Z. 2000, *ApJ*, 534, 324
- Knapp, G. R., Young, K., Lee, E. & Jorissen, A. 1998, *ApJS*, 117, 209
- Kwok, S. 1993, *ARA&A*, 31, 63
- Kwok, S., Volk, K. & Hrivnak, B. J. 1999, *A&A*, 350, L35
- Le Bertre, T. 1997, *A&A*, 324, 1059
- Meixner, M., Skinner, C. J., Graham, J. R., Keto, E., Jernigan, J. G., & Arens, J. F. 1997, *ApJ*, 482, 897
- Meixner, M. et al. 1999, *ApJS*, 122, 221
- Olofsson, H., Bergman, P., Lucas, R., Eriksson, K., Gustafsson, B., & Bieging, J. H. 2000, *A&A*, 353, 583
- Parthasarathy, M., Garcia Lario P., & Pottasch, S. R. 1992, *A&A*, 264, 159
- Reimers, C., Dorfi, E. A. & Hofner, S. 2000, *A&A*, 354, 573
- Schroder, K.-P., Winters, J. M. & Sedlmayr, E. 1999, *A&A*, 349, 898
- Soker, N. 1998, *MNRAS*, 299, 1242
- Soker, N. & Clayton, G. C. 1999, *MNRAS*, 307, 993

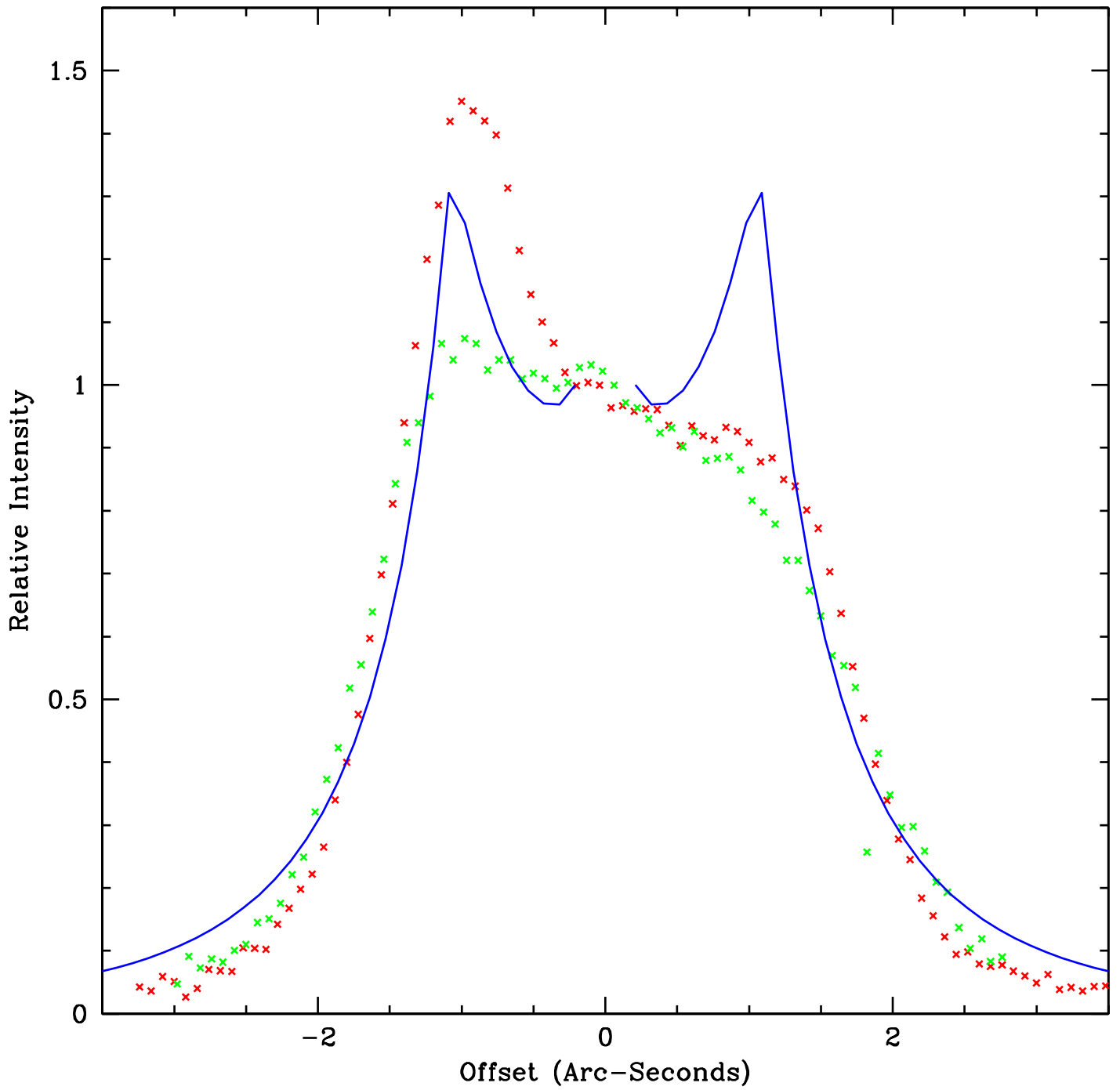
- Sopka, R. J., Hildebrand, R., Jaffe, D. T., Gatley, I., Roellig, T., Werner, M. Jura, M., & Zuckerman, B. 1985, ApJ, 294, 242
- Tuchman, Y., Lebre, A., Mennessier, M-O., & Ya'ari, A. 1993, A&A, 271, 501
- Ueta, T., Meixner, M. & Bobrowsky, M. 2000, ApJ, 528, 861
- Vassiliadis, E. & Wood, P. R. 1993, ApJ, 413, 641
- von Helden, G., Tielens, A. G. G. M., van Heijnsbergen, D., Duncan, M. A., Hony, S., Waters, L. B. F. M. & Meijer, G. 2000, Science, 288, 313
- Wiebe, D. S. & Watson, W. D. 1998, ApJ, 503, L71
- Van Winckel, H. & Reyniers, M. 2000, A&A, 354, 135
- Winters, J. M., Fleischer, A. J., Le Bertre, T., & Sedlmayr, E. 1997, A&A, 326, 305

### FIGURE CAPTIONS

Fig 1. The  $11.7 \mu\text{m}$  image of HD 56126. North is to the top and East is to the left; these directions are displayed on the Figure by lines whose lengths are  $1''$  each. The maximum surface brightness that we detected and shown in the red color is  $4.0 \text{ Jy arcsec}^{-2}$ . The yellow, green and purple colors correspond to 2.4, 1.6 and  $0.40 \text{ Jy arcsec}^{-2}$ , respectively.

Fig. 2. Two cuts through the  $11.7 \mu\text{m}$  image of HD 56126. Red and green crosses are used for tracing the images at position angles of  $135^\circ$  and  $45^\circ$ , respectively, while the results from the spherically symmetric model are plotted as a solid blue line.





This figure "HD56126.jpg" is available in "jpg" format from:

<http://arxiv.org/ps/astro-ph/0010038v1>